The 2013 World Congress on
Advances in Nano, Biomechanics, Robotics, and Energy Research (ANBRE13)
Seoul, Korea, August 25-28, 2013

Cat Landing on Rigid and Flexible Surfaces: Semi-Flat Multi Impact Modeling and Path Planning in Presence of Constraints

*Ali Meghdari[1)] and S.M.Hadi Sadati[2)]

[1), 2)] *Department of Mechanical Engineering, Sharif U.T., Tehran 11365-11155, Iran*
[1)] meghdari@sharif.edu

ABSTRACT

Three-phase landing for a 7-links 2D cat model is studied using semi-flat dynamic and force-control methods on rigid and flexible surfaces, considering switching constraints and a spring-damper model on impact points respectively, in presence of rotational angle, velocity, torque constraints and control signal delay. The landing phases are: pre-landing in which the robot adopts the optimal configurations to absorb the in-joint impulses, single-contact in which the robot settles on one pair of its limbs, and double-contact in which the second pair impacts the ground. In each step, desired inputs are derived using semi-flat equations so that the body center of mass trajectory and free limbs' maneuver can guarantee the model stability and maintain desired impact forces in contacting points. Newtonian equations are considered to account for states' change in all rapid foot-ground impacts and resulting in-joint impulses. In-joint contacts due to reaching rotational limits are modeled using a simple switching method. Finally the proposed path planning method efficiency in high jumps is investigated through simulations and it is showed that despite the easier dynamic modeling of the flexible surface idea and its more generality, the input generation using dynamic inversion is more difficult and less accurate in this case.

1. INTRODUCTION

Motion dynamics of cat species has always been attractive to be studied. Flexibility in motion due to specific skeleton and complex muscle-skeleton mechanism, control concepts, special way of running, high speed direction change while moving, ability of twisting the body during free fall, and landing on four limbs were investigated in literature and the results have been used in different branches such as control, robotics and aerospace. Reducing impulses while maintaining stability, damping pre impact kinetic energy and reducing linear momentum are important facts in landing of a cat jump. This is similar to air vehicles, space ships, parachute or athletes'' landing. Controlling maximum in-joint or contact point impulses by deforming the body, such as bending knees and lowering upper body in a human high jump landing, is called soft landing [1] which needs specific maneuver path planning.

[1)] Professor
[2)] Graduate Student

Despite vast publications on human beings, investigating landing dynamic of cat species and other animals is quite rare in literature. The only publications on cats are experiments on muscle reflection in high jump landing to explore muscle specifications and not the maneuver dynamics ,[2]. Reback showed that cat muscles become active 30 ms before contact, however landing maneuver is the same for different jump heights from 0.4 to1 m with different joints' angular velocities [3]. Agile dog landing experiments focusing on their injury prevention [4] and a frog conceptual design able to jump and land based on the real animal dynamics without considering impulses in Harbin university are the most relevant publications concerning other animals landing motion. Human landing biomechanics [5], athletes' touchdown dynamics [6] using dynamic models or finite element methods [7], and fall detection and injury prevention for elderlies [8-10] are widely studied. Explorations on human falling impacts modeling [11] and athletes' landing optimum path planning and configuration [12-14] specially for gymnasts [9, 15, 16] are similar to the proposed topic in this research. Furthermore, parachute touchdown planning studied experimentally in [17] is another similar research on human landing. It is shown that considering soft tissue and deformable bones affect landing impulses in human beings using wobbling mass model. It also predicted that impact forces and accelerations are 1.5 to 2 times less than a rigid model which is in better agreement with real experiments [8, 16]. More complete models consider stiffening of muscles before the impact [8, 14] by reducing the wobbling mass amount [16]. The soft tissue effects are not considered in our model, since the results are based on a rigid cat robot, not a real animal.

Considering impact impulses as the main injury cause was route to defining hard and soft human landing methods such as trainings in free running with large waist and leg bending, and firm no joint bend maneuver in gymnastic respectively [18]. Filling lungs with air as an insufficient method of decreasing impulses [19] and increasing body weight effect on these impacts [20] are investigated as well. It is showed that in a common height jump the landing impulses exceeds to 4.5 times the body weight for agile dogs [4] and 2.9 to3.4 times for a human being [7]. Maximum of 8 to 14.4 times the body weight is reported for athletes and gymnasts [8].

Rok So's study in 2004 using ZMP method of stability analysis, in-joint impulses investigation and dynamic inversion method of path planning of a three phase 2D gymnast's landing model is one of the most comprehensive studies in this field [10] which is completed by Sheets by adding hands in 2007 [16]. Some human running investigations consider a continuous jump and 2D spring-mass landing model which can be a source of inspiration here too ,[21].

Landing and contact impulses analysis in robotics are studied for spaceship entry missions on other planets (especially mars) ,[22], some bio-inspired jumping robots [1, 23-25], hopping robots [1], and humanoid walking robots stability [26], and fall injury prevention [27]. Wong's 2D four legs robot landing model uses inverse jump kinematics to plan landing path for kinetic energy damping and suggests high speed evaluation of a simple model to account for the best leg-ground angle in impact instance in order to minimize the landing impulses and ground forces [24]. Yamakita represents a switching control based on a two legs gymnast robot touchdown condition and configuration [25]. Sato introduced a set of input signals to reduce the contact point relative velocity w.r.t. surface as the leg moves toward the ground to control contact impulses [1, 28].

Furthermore, it is shown that reducing in-joint impulses in weakest direction which is usually perpendicular to the elements' longest axis is more important than contact point impulses [10]. While most of the studies do not consider continuous impacts in landing touch down or represent a complicated model for that in running dynamic models, Tedrake represents a Lagrangian dynamic model for a running robot on a rigid surface using a switching constraint to model the contact and separation of the leg tips without impact analysis in combination with a forward optimization method for motion path planning [29]. Rigid surface Modeling means no penetration of the contact points and considering a pivot joint in contact place which will results in more continuous impacts before the settlement [10, 23, 29], while in a deformable spring-damper surface model the resulting forces are related to contact point penetration to the ground [1, 12, 30]. Rigid models are used for running analysis while the deformable one are widely used in landing and impact analysis and accurate contact simulations for medical force control applications [6, 31, 32].

In-joint impulses are torques and force impulses exerts in constrained direction of free joints [10] and derived based on integration of close formulation of Newtonian EOM of separate elements [31]. Pain modeled a gymnast landing on a deformable surface, considering wobbling masses, deformable bones and in-joint impulses and showed minimizing in-joint impulses are more important [12]. It is also showed that ankle and knee joints absorb more energy than waist in human soft landing [20].

Unfortunately, there is no comprehensive modeling and path planning study on high jump landing maneuver of animals such as cats considering essential effects of Continuous impacts and in-joint impulses aiming to build a real robotic model. Since side forces are small in four legs animals landing [9], in this research, the maneuver dynamic modeling and path planning for a 7 links 2D model from first foot pair ground contact through its complete settlement are studied using a three phase model. The landing phases are: pre-landing in which the robot adopts the optimal configurations to reduce the in-joint impulses efficiently with a sudden activation of joint motors and absorb more kinetic energy in subsequent phases, single-contact in which the robot settles on one pair of its limbs and lasts until the second legs' pair tips reach the ground, and double-contact in which the second pair impacts the ground and the robot momentum is decreased in a planned manner to reduce contact forces of the legs. Continuous and exact impact modeling of legs' tip and joints on a rigid surface and a deformable surface model, and easy to derive and implement matrix method for dynamic modeling and dynamic inversion path planning, called TMT method, are the main features of this research.

Although the cat free fall is not considered in this research [33], in pre impact phase, optimal angles for the spatial rotation of the model front body have been found using direct optimization. In contact instance, desired joint motors' input are derived using semi-flat model to satisfy desired goals and assumed constraints in order to lower the impact impulses by reducing contact leg tip absolute speed relative to the surface. Newtonian impact equation accounts for contact point impulses and after impact velocities while the model configuration remains unchanged. In single contact phase, for rigid surface model a switching constrained dynamic method, and for deformable surface model a spring-damper method is considered. The model is assumed to be in contact while lags are touching the ground and ground normal force is positive. So leg-

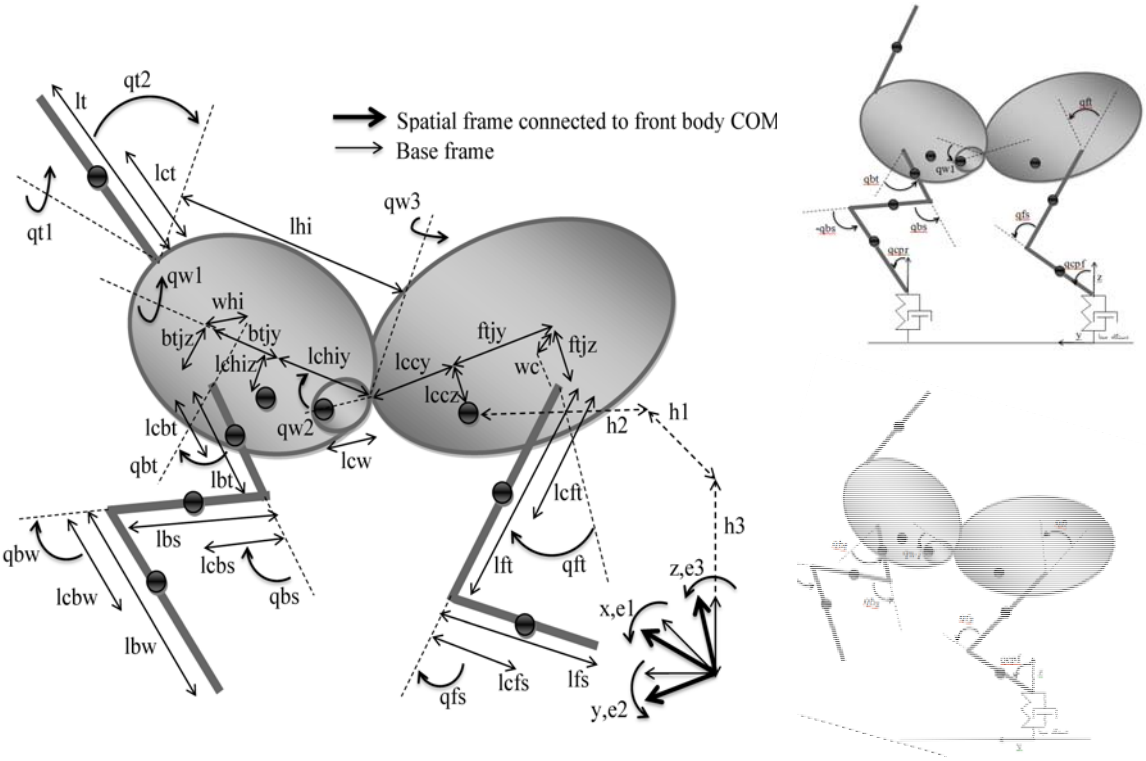

Figure 1. 7 links 2D cat model in (top); Deformable surface model in single and multi-contact phase (down)

ground separations are monitored and every velocity changes due to re-contacts are calculated using the Newtonian equations. Reaching floating leg tip to the ground with zero velocity vector, maintaining stability considering static stability index and lowering contact point force vector instantly to the model static weight are the goal constraints in input signal generation in this phase. Reaching joints' configuration and velocity limits are modeled by switching a constraint on and off, to stop their rotations and velocity increases respectively, without any impact modeling. Double contact phase started as the second leg pairs reach the ground. Here it does not mean that both feet are in contact with the surface since they might be on fly due to a previous impact. However the goal constraints in the path planning method is changed to reduce both contact point force vectors and lower the model center of mass position and velocity (COM) in a smooth manner to settle the model. Goal constraints on force vectors are derived so the legs' tip which is not in contact tends to reach the surface as fast as possible. Furthermore the reduced degree of freedom (DOF) due to double contact in rigid surface model is considered which is not encountered in the deformable surface. The two first phases' equations of motions (EOM) have some minor differences with in which leg pairs that contact first are reflected.

The results of this study is a comprehensive model and exact path planning method which can be implemented in a real cat robot, and as an inspiration for similar research on human fall, athletes' and parachute touchdown, and other kinds of robots and space ship landing and path planning as well. It considers various control, configuration, sensory and motor limitations in a real application by means of a simple easy to use switching constrained matrix dynamic model.

2. Modeling

2.1 7 links 2D Cat Model

Figures 1 shows the 7 links 3D model and Deformable surface single and multi-contact phase respectively. For the free fall model the spatial frame is attached to the front body at its COM position (the natural position of gyroscope sensor.) Free fall model parameters are as in [33] derived using a pre-conceptual model of a cat robot based on the animal anatomy [34] and MIT Cheetah model [35] using SolidWorks software, but are not necessarily as the real values in a natural cat (Table (1)). Considering the cats' typical hands' movement and for simplicity in the distributed model analysis, the rear hands' wrist angle considered to be equals to rear hands' shank angle and in opposite signs. Tail is fixed upright too. Shank angles stops and do not follow the above relation as they reach their limits. The free fall phase is modeled as in [33] and not repeated here.

2.2 Motion Dynamical Modeling (TMT)

Constrained Rigid Surface Model A matrix form of EOM Eq. (1) using TMT method in Eq. (2) is used to derive dynamic models ,[36, 37]. $\bar{\boldsymbol{M}}$, $\boldsymbol{T}_{\mathrm{cn}}$, $\boldsymbol{q}$, $\boldsymbol{\lambda}$, $\boldsymbol{d}_{\mathrm{EOM}}$ and $\boldsymbol{d}_{\boldsymbol{\lambda}}$ are inertial and mass matrix in Lagrange equations, constrained generalized velocities coefficients matrix, generalized coordinates vector, Lagrange multipliers vector, vector of other terms in Lagrange equation, and vector of other terms in constraint equation derivative respectively. Constraints are differentiated multiple times, so their order of differentiation equals that of the EOM, which is 2 here [38].

$$\begin{bmatrix} \bar{\boldsymbol{M}} & \boldsymbol{T}_{\mathrm{cn}}^{\mathrm{T}} \\ \boldsymbol{T}_{\mathrm{cn}} & \boldsymbol{0} \end{bmatrix} \cdot \begin{bmatrix} \ddot{\boldsymbol{q}} \\ -\boldsymbol{\lambda} \end{bmatrix} = \begin{bmatrix} \boldsymbol{d}_{\mathrm{EOM}} \\ \boldsymbol{d}_{\boldsymbol{\lambda}} \end{bmatrix} \tag{1}$$

Using this forms of EOM enable us to implement numerical matrix inverse methods simply and derive the vector of unknowns ($[\ddot{\boldsymbol{q}} \quad -\boldsymbol{\lambda}]^{(\mathrm{T})}$) in all of this research sections.

TMT Method TMT method is a simple, clear and optimum method which eliminates the highest order derivatives in each step and results in a simplified matrix form of unconstrained EOM, ideal for numerical calculation of complex and large dynamic systems. Here $\boldsymbol{T}$, $\boldsymbol{M}$, $\boldsymbol{m_i}$, $\boldsymbol{I_i}$, $\boldsymbol{f}$ and $\boldsymbol{Q}_{\mathrm{nc}}$ are transformation matrix for multi body links' COM position and rotation in terms of generalized coordinates, system's mass and inertia matrix, i^{th} link mass and inertia matrix, and conservative and non-conservative forces' virtual work vector respectively. Jacobian operator order and independent variables of each vector or matrix function are shown using an Einstein like notation [36, 37].

$$\begin{aligned} &\overline{\boldsymbol{T}} = \boldsymbol{T}_{(\boldsymbol{q}),(\boldsymbol{q})}, \qquad \boldsymbol{d} = \left(\overline{\boldsymbol{T}}\dot{\boldsymbol{q}}\right)_{,(\boldsymbol{q})}, \qquad \dot{\boldsymbol{q}} = \boldsymbol{T}_{(\boldsymbol{q}),(\boldsymbol{q},\boldsymbol{q})}\dot{\boldsymbol{q}}\dot{\boldsymbol{q}}, \\ &\boldsymbol{M} = \mathrm{diag}\left[\boldsymbol{m}_1\boldsymbol{m}_1\boldsymbol{m}_1\boldsymbol{I}_{1[\mathbf{3}\times\mathbf{3}]} \cdots\right], \qquad \bar{\boldsymbol{M}} = \overline{\boldsymbol{T}}^{(\mathrm{T})}\boldsymbol{M}\overline{\boldsymbol{T}}, \\ &\boldsymbol{d}_{\mathrm{EOM}} = \overline{\boldsymbol{T}}^{(\mathrm{T})}\left[\sum \boldsymbol{f} - \boldsymbol{M}\boldsymbol{d}\right] + \boldsymbol{Q}_{\mathrm{nc}}, \qquad \bar{\boldsymbol{M}}\ddot{\boldsymbol{q}} = \boldsymbol{d}_{\mathrm{EOM}}. \end{aligned} \tag{2}$$

Deformable Surface Model Deformable surface model needs no constraint on contact points and forces due to parallel spring-damper system deformation, which are fixed in one end to a rigid base and the other end to leg tip, are exerted on these points.

2.3 Impact Model

Newtonian Impact model Sudden change in velocities (generalized coordinates differentiates) due to impact while the configuration remains unchanged, derived by solving two Newtonian impact equations [10] which are based on integration of model EOM on the impact infinitesimal duration, and relative after and before impact velocity vectors for contact point w.r.t. surface (Eq. (3)) [36, 37]. $\boldsymbol{T}_{\mathrm{cp}}$, $\dot{\boldsymbol{q}}^{(\pm)}$, $\boldsymbol{\rho}$ and $\boldsymbol{E}$ are transformation matrix for contact point position vector in terms of generalized coordinates, after and before contact generalized vector differentiate, contact impulse vector and diagonal matrix of impact coefficients.

$$\begin{matrix}\boldsymbol{T}_{\mathrm{cp}}\dot{\boldsymbol{q}}^{(+)} = -\boldsymbol{E}.\boldsymbol{T}_{\mathrm{cp}}.\dot{\boldsymbol{q}}^{(-)} \\ \boldsymbol{M}.\dot{\boldsymbol{q}}^{(+)} + \boldsymbol{T}_{\mathrm{cp}}^{(\mathrm{T})}.\boldsymbol{\rho} = \boldsymbol{M}.\dot{\boldsymbol{q}}^{(-)}\end{matrix} \quad \rightarrow \quad \begin{bmatrix}\boldsymbol{M} & \boldsymbol{T}^{(\mathrm{T})}{}_{\mathrm{cp}} \\ \boldsymbol{T}_{\mathrm{cp}} & 0\end{bmatrix}\begin{bmatrix}\dot{\boldsymbol{q}}^{(+)} \\ \boldsymbol{\rho}\end{bmatrix} = \begin{bmatrix}\boldsymbol{M}.\dot{\boldsymbol{q}}^{(-)} \\ -\boldsymbol{E}.\boldsymbol{T}_{\mathrm{cp}}\dot{\boldsymbol{q}}^{(-)}\end{bmatrix} \tag{3}$$

In-joint impulses In-joints' force and torque impulses for each body can be found by integrating a close Newtonian formulation of separate links' EOM as in [31]. Substituting contact point impulses and before and after generalized coordinates differentiations using Eq. (3) and zero value for free ends' impulses in Eq. (4), one can solve equations for joint impulses. Here $\pm$ superscripts mean after and pre impact values and $m_{[j]}$, ${}^{\mathrm{b}}_{\mathrm{c}}\boldsymbol{I}_{[j]}$, ${}^{\mathrm{b}}_{\mathrm{c}}\boldsymbol{r}_{[j]}$, $\Delta\,{}^{b}\boldsymbol{\omega}_{[j]}$, $\Delta^{b}_{b}\boldsymbol{v}_{c[j]}$, ${}^{b}\boldsymbol{\rho}_{\tau[j]}$, ${}^{b}\boldsymbol{\rho}_{f[j]}$, $\boldsymbol{\rho}_{f\tau}$, $\boldsymbol{q}^{\pm}$, $\boldsymbol{B}_{\mathrm{ii}}$ and $\boldsymbol{i}_{\mathrm{dcrf}}$ are i^{th} link mass, inertia, joint position vector relative to link COM represent in base reference coordinate, rotational and linear velocity sudden change before and after impact, joint torque and force impulses, impulse vector, pre and post impact generalize coordinates as in Fig. (1), near diagonal matrix with ± 1 elements for effective impulses on each link set of equations, and contact point impulse vectors calculated from Eq. (3).

$$m_{[j]}.\Delta^{b}_{b}\boldsymbol{v}_{c[j]} = -\,{}^{b}\boldsymbol{\rho}_{f[j]} + {}^{b}\boldsymbol{\rho}_{f[j+1]} \tag{4}$$

$$\begin{matrix}{}^{\boldsymbol{b}}_{\boldsymbol{c}}\boldsymbol{I}_{[j]}.\Delta\,{}^{b}\boldsymbol{\omega}_{[j]} = -\,{}^{b}\boldsymbol{\rho}_{\tau[j]} + {}^{b}\boldsymbol{\rho}_{\tau[j+1]} - {}^{b}_{c}\boldsymbol{r}_{[j]}.\,{}^{b}\boldsymbol{\rho}_{f[j]} + {}^{b}_{c}\boldsymbol{r}_{[j+1]}.\,{}^{b}\boldsymbol{\rho}_{f[j+1]} \\ \rightarrow -\boldsymbol{M}^{-}\boldsymbol{T}^{-}\dot{\boldsymbol{q}}^{-} + \boldsymbol{M}^{+}\boldsymbol{T}^{+}\dot{\boldsymbol{q}}^{+} = \boldsymbol{B}_{\mathrm{ii}}\boldsymbol{\rho}_{f\tau} + \begin{bmatrix}\boldsymbol{0} \\ \boldsymbol{i}_{\mathrm{dcrf}}\end{bmatrix}\end{matrix}$$

Here the torque impulses. exerted on motors, are not evaluated. For a double contact impact, both leg pairs' impulse vectors should be substitute as $\boldsymbol{i}_{\mathrm{dcrf}}$.

3.4 Semi-Flat Equations

A system is flat or differentially flat when all the states and inputs can be found as functions of outputs and a limited number of their derivatives with bounded orders. These outputs are named "flat outputs". It results in finding exact inputs for any desired outputs, which is somehow similar to output-input linearization method in nonlinear

control, and hence considered as a geometric approach to path planning problems [39]. Despite lack of generality, its advantages are in path planning by reducing the order and/or complexity of the optimized path planning problems as they find suitable output functions instead of inputs. Recently new investigations showed the sufficient conditions of finding such outputs for all kinds of under actuated systems, [40]; however its applicability and method of deriving the flat output for all kind of systems are open problems. Here we define a system as semi-flat if a bounded order of states' and input functions' derivatives can be found as a function of lower order inputs' or states' functions' derivatives, outputs' function, and a limited number of their derivatives with bounded orders Eq.(5) which is shown to be more general than the definition of flat systems. This definition results in a set of ordinary differential equations (ODE) for states' and inputs' functions which are hard to solve analytically but with an appropriate numerical integration method the time series of exact inputs to generate any desired outputs' functions can be found which is similar to dynamic inversion methods. Here $\boldsymbol{x}$, $\boldsymbol{u}$ and $\boldsymbol{y}$ are state, input and output vectors and α, β and γ are derivations' order respectively.

$$\begin{aligned} \boldsymbol{x}^{[\beta]} &= \boldsymbol{a}(\boldsymbol{x}, \dots, \boldsymbol{x}^{[\beta-1]}, \boldsymbol{u}, \dots, \boldsymbol{u}^{[\gamma-1]}, \boldsymbol{y}, \dots, \boldsymbol{y}^{[\alpha]}) \\ \boldsymbol{u}^{[\gamma]} &= \boldsymbol{b}\left(\boldsymbol{x}, \dots, \boldsymbol{x}^{[\beta-1]}, \boldsymbol{u}, \dots, \boldsymbol{u}^{[\gamma-1]}, \boldsymbol{y}, \dots, \boldsymbol{y}^{[\alpha]}\right) \end{aligned} \tag{5}$$

2.4. Constraints

System limitations Constraints are one of the main sources of nonlinearity in a system such as saturation in actuators and sensors, dead zone, clearance, etc. Here a simple saturation function is used to model the geometrical, kinematical and dynamical constraints. Besides methods of discrete integration is used whenever a signal time delay is encountered as in control update period. Aside joints' rotation angle limits due to geometrical design, since a set of Dynamixel R-64 servo motors are considered for the real model, a control delay, angular velocity and torque limit of 0.01 [s], ±6.4 [rad/s] and ±1.67 [Nm] are considered in modeling respectively {#625).

Goal Functions (Constraints) In semi-flat model or inverse dynamic of a system, goal constraints are desired values for nonlinear equalities that combine with solving EOM and results in finding exact input signals to steer the system to a pre-defined behavior. These functions can be implement as common constraint functions (Eq. (6)). Here $\boldsymbol{g}(\boldsymbol{q})$, $\boldsymbol{g}_{\mathrm{d}}$, $\boldsymbol{g}_t$, $\boldsymbol{T}_{\mathrm{d}}$, $\boldsymbol{u}_{\mathrm{d}}$ and $\boldsymbol{a}_{\mathrm{d}}$ (or $\boldsymbol{d}_{\mathrm{d}}$) are goal function vector in terms of generalized coordinates, final and current qoal function vector value, transformation matrix for desired function vector in terms of generalized coordinates, desired output, and desired acceleration vector of reaching the goal function from its current value. Here we approach toward the desired values with constant acceleration of which one tends to reach the goal with zero state differentiate (velocity) while the other one approaches it in an infinitesimal time (ts or h) as follows.

$$\boldsymbol{g}(\boldsymbol{q}) = \boldsymbol{g}_{\mathrm{d}} \rightarrow \boldsymbol{T}_{\mathrm{d}}\dot{\boldsymbol{q}} = \boldsymbol{u}_{\mathrm{d}} \rightarrow \boldsymbol{T}_{\mathrm{d}}\ddot{\boldsymbol{q}} + \left(\boldsymbol{T}_{\mathrm{d}(\boldsymbol{q})}\dot{\boldsymbol{q}}\right)\dot{\boldsymbol{q}} = \boldsymbol{a}_{\mathrm{d}} \tag{6}$$

$a_{\mathrm{d}} = -\frac{{u_{d[3]}}^2}{2\times(g_{\mathrm{d}}-g_t)}$: Smooth approach toward goal with final zero velocity

$$a_{\mathrm{d}} = 2 \times \frac{(g_{\mathrm{d}} - g_t) - u_d \times ts}{ts^2}$$: Time fixed approach toward goal

3. Formulation and Path Planning

Nakano defined soft landing as minimizing contact impulses in impact instance, and lowering contact forces as the kinetic energy rejects to settle {#245}. Here the main method for path planning is semi-flat dynamic, while different goal constraint are considered for each landing model and phase.

3.1 Pre Impact Phase

Newtonian Contact Equation Here an optimal angle for the model's front body inclination angle w.r.t. surface has been investigated using direct optimization. The limbs are open to have full range damping effect for the subsequent phases, and thigh and shank have 3 degrees absolute inclination each, placing the straightened legs as perpendicular as possible to the ground and under the body to minimize the in-joint harmful impulses which excreted perpendicular to limbs axis. The waist bends 84 degrees inward to minimize these impulses too, and front body spatial angle is considered as the only optimization DOF. The weak axis for the shoulders is parallel with the front and rear body horizontal axis. In contact instance, desired joint motors inputs to reduce the contact leg tip relative speed to the surface is found using dynamic inversion considering joint and motor limits, since the Newtonian impact model predicts the least contact impulse if the reaching relative speeds become zero.

Matrix form of Eq. (3) is used and after and before contact generalized coordinates' differentiation and contact impulses considered as the unknowns (Eq. (7)). Model COM linear velocity vector is known, and the following five goal constraints are used to solve the inverse dynamic: 1 & 2) contact point velocity vector equals zero to reduce impulses and slipping probability, 3 & 4) impulse vector equivalents to the body weight (an impulse control feature), 5) waist joint is fixed with zero velocity and the goals would be achieved by actuating other four joints. The before contact states differentiations should not exceed joints' rotational velocity limits and this is guaranteed by checking the results and fixing the joints' before contact velocity for the not satisfactory values. The procedure of re-evaluating the contact equation and constraint limit check continues so all the inputs are found in their saturation limits. Constraining each joint velocity on one of its saturation boundary values, needs omitting one of the five goal constraints and this starts from the fifth one to the first one in the so called order. Final results for pre impact input signals may not satisfy none of the goal functions completely; however it would be the nearest possible result. Here $\boldsymbol{rcm}$, $\boldsymbol{rcp}$, $\boldsymbol{H}_{\mathrm{eqhc}[3\times13]}$, $\boldsymbol{v}^{-}_{\mathrm{cm}[3\times1]}$, g and h are COM vector in pre impact model, contact point vector in post impact model, non-holonomic constraints coefficients matrix for free fall pre impact model as in [33], pre impact COM velocity vector, gravitational acceleration and primary COM falling height. The last five rows of the equations are the goal constraints.

It can be seen that the dimension of $\boldsymbol{M}$ should be equals in pre and post impact model (which is 42 since the pre impact model is a 3D model as in [33] with 6 DOF for each of 7 links.) while the generalized coordinates' vectors' dimension can be varied.

$$\begin{bmatrix} \widehat{\boldsymbol{M}}^{+}{}_{[8\times8]} & \boldsymbol{T}_{\mathrm{cp}}{}^{+(\mathrm{T})}{}_{[8\times2]} & \widehat{\boldsymbol{M}}^{-}{}_{[8\times11]} \\ \boldsymbol{T}_{\mathrm{cp}}{}^{+}{}_{[2\times8]} & \boldsymbol{0} & \boldsymbol{E}_{[2\times2]}.\boldsymbol{T}_{\mathrm{cp}}{}^{-}{}_{[2\times11]} \\ \boldsymbol{0} & \boldsymbol{0} & \boldsymbol{H}_{\mathrm{eqhc}[3\times11]} \\ \boldsymbol{0} & \boldsymbol{0} & \boldsymbol{0}_{[3\times8]}\ \boldsymbol{I}_{[3\times3]} \\ \boldsymbol{0} & \boldsymbol{0} & \boldsymbol{T}_{\mathrm{cp}}{}^{-}{}_{[2\times11]} \\ \boldsymbol{0} & \boldsymbol{0} & \boldsymbol{0}_{[2\times3]}\ 1\ \boldsymbol{0}_{[2\times7]} \\ \boldsymbol{0} & \boldsymbol{I}_{[2\times2]} & \boldsymbol{0} \end{bmatrix}_{[21\times21]} \begin{bmatrix} \dot{\boldsymbol{q}}^{+}{}_{[8\times1]} \\ \boldsymbol{\rho}_{[2\times1]} \\ \dot{\boldsymbol{q}}^{-}{}_{[11\times1]} \end{bmatrix}_{[21\times1]} = \begin{bmatrix} \boldsymbol{0} \\ \boldsymbol{0} \\ \boldsymbol{d}_{\mathrm{d}[11\times1]} \end{bmatrix}_{[21\times1]} \tag{7}$$

$$\boldsymbol{d}_{\mathrm{d}[10\times1]} = \begin{bmatrix} \boldsymbol{0}_{[3\times1]} \\ \boldsymbol{v}^{-}_{\mathrm{cm}[3\times1]} \\ \boldsymbol{0}_{[5\times1]} \end{bmatrix}_{[11\times1]}, \qquad \boldsymbol{v}^{-}_{\mathrm{cm}[3\times1]} = \begin{bmatrix} 0 \\ 0 \\ -\sqrt{2.\mathrm{g}.h} \end{bmatrix}$$

$$\widehat{\boldsymbol{M}}^{\pm}{}_{[8\times8\ or\ 11]} = \overline{\boldsymbol{T}}^{+(\mathrm{T})}_{[8\times42]}\boldsymbol{M}_{[42\times42]}\overline{\boldsymbol{T}}^{\pm}_{[42\times11\ or\ 8]}$$

$$\boldsymbol{q}^{-} = [\boldsymbol{e}_{[1]}\quad \boldsymbol{e}_{[2]}\quad \boldsymbol{e}_{[3]}\quad \boldsymbol{qw}_{[2]}\quad qft\quad qfs\quad qbt\quad qbs\quad \boldsymbol{rcm}_{[1]}\quad \boldsymbol{rcm}_{[2]}\quad \boldsymbol{rcm}_{[3]}]^{(\mathrm{T})}{}_{[1\times11]}$$

$$\boldsymbol{q}^{+} = [qc\quad qft\quad qfs\quad qw1\quad qbt\quad qbs\quad \boldsymbol{rcp}_{[1]}\quad \boldsymbol{rcp}_{[2]}]^{(\mathrm{T})}{}_{[1\times8]}$$

In-joint Impulses As in Eq. (4), the in-joint impulse matrix form is derived as in Eq. (8). Here all the 42 DOF of elements presents, however the only 14 linear impulsive force elements in 2D plane is of concern which four of them are contact point impulses, two of which are calculated from Eq. (8) and the other two equal zero for the free leg pair tip. The elements with none zero values of ±1 in $\boldsymbol{B}_{\mathrm{ii}}$ are shown with their column number along with their appropriate sign. Then the perpendicular and parallel impulses to each element at each joint ($\boldsymbol{\rho}_{pp}$) is calculated by multiplying a matrix of absolute rotation (calculated below) of that element ($\boldsymbol{R}_{??}$). Here $\boldsymbol{i}_{\mathrm{dcff}}$ and $\boldsymbol{i}_{\mathrm{dcrf}}$ are front and rear leg pair tip impulse vectors, and r subscript stands for absolute rotational angles.

$$-\boldsymbol{M}^{-}_{[14\times14]}\boldsymbol{T}^{-}_{[14\times11]}\dot{\boldsymbol{q}}^{-}_{[11\times1]} + \boldsymbol{M}^{+}_{[14\times14]}\boldsymbol{T}^{+}_{[14\times8]}\dot{\boldsymbol{q}}^{+}_{[8\times1]} = \boldsymbol{B}_{\mathrm{ii}[14\times14]}\boldsymbol{\rho}_{[14\times1]} + \begin{bmatrix} \boldsymbol{i}_{\mathrm{dcff}[2\times1]} \\ \boldsymbol{0}_{[10\times1]} \\ \boldsymbol{i}_{\mathrm{dcrf}[2\times1]} \end{bmatrix}_{[14\times1]} \tag{8}$$

$$\boldsymbol{B}_{\mathrm{ii}} = \begin{bmatrix} 5 & -7 \\ 6 & -8 \\ 7 & -9 \\ 8 & -10 \\ 3 & -5 \\ 4 & -6 \\ 1 & -3 \\ 2 & -4 \\ 9 & -11 \\ 10 & -12 \\ 11 & -13 \\ 12 & -14 \\ 13 & 0 \\ 14 & 0 \end{bmatrix}_{[14\times14]}, \qquad \boldsymbol{\rho}_{pp} = \begin{bmatrix} \boldsymbol{R}_{\mathrm{fs}} & & & & & & & & & & & & & \\ & \boldsymbol{R}_{\mathrm{fs}} & & & & & & & & & & & & \\ & \boldsymbol{R}_{\mathrm{ft}} & & & & & & & & & & & & \\ & & \boldsymbol{R}_{\mathrm{ft}} & & & & & & & & & & & \\ & & \boldsymbol{R}_{\mathrm{c}} & & & & & & & & & & & \\ & & & \boldsymbol{R}_{\mathrm{c}} & & & & & & & & & & \\ & & & \boldsymbol{R}_{\mathrm{hi}} & & & & & & & & & & \\ & & & & \boldsymbol{R}_{\mathrm{hi}} & & & & & & & & & \\ & & & & \boldsymbol{R}_{\mathrm{bt}} & & & & & & & & & \\ & & & & & \boldsymbol{R}_{\mathrm{bt}} & & & & & & & & \\ & & & & & \boldsymbol{R}_{\mathrm{bs}} & & & & & & & & \\ & & & & & & \boldsymbol{R}_{\mathrm{bs}} & & & & & & & \\ & & & & & & & \boldsymbol{R}_{\mathrm{bw}} & & & & & & \end{bmatrix}_{\mathrm{ffc}[26\times14]} \cdot \boldsymbol{\rho}_{[14\times1]}$$

$$\boldsymbol{\rho}_{[14\times1]} = \begin{bmatrix} fc_{\mathrm{y}}\text{: Front body} \\ fc_{\mathrm{x}} \\ hi_{\mathrm{y}}\text{: Hip} \\ hi_{\mathrm{z}} \\ ft_{\mathrm{y}}\text{: Front thigh} \\ ft_{\mathrm{z}} \\ fs_{\mathrm{y}}\text{: Front shank} \\ fs_{\mathrm{z}} \\ bt_{\mathrm{y}}\text{: Back thigh} \\ bt_{\mathrm{z}} \\ bs_{\mathrm{y}}\text{: Back shank} \\ bs_{\mathrm{z}} \\ bw_{\mathrm{y}}\text{: waist} \\ bw_{\mathrm{z}} \end{bmatrix}_{[14\times1]}, \quad \begin{matrix} \text{Absolute element angles:} \\ qcpr = qcp \text{ (Contact point)} \\ qfsr = qcp \text{ (Front shank)} \\ qftr = qcp + qfs \text{ (Front thigh)} \\ qcr = qcp + qfs + qft \text{ (Front body)} \\ qhr = qcr + qw \text{ (Hip)} \\ qbtr = qhr + qbt = qbwr \text{ (Back thigh)} \\ qbsr = qbtr + qbs \text{ (Back shank)} \end{matrix}$$

Here a weighted summation of COM position divided by the mean leg pairs tips horizontal position as an index for static stability, contact velocity vector, and summation of in-joint harmful impulses are considered as the optimization criteria of finding appropriate front body inclination angle w.r.t. surface.

3.2 Single Contact Phase

Rigid Surface Model From now one joints' motor input torques are considered as the unknowns ($\boldsymbol{\tau}$) and goal functions are used to determine the desired torque and joints' instance rotational velocities (Eq. (9)). Here the five goal constraints are 1) Free leg thigh becomes vertical w.r.t. surface as fast as possible (in an infinitesimal time), 2) contact point normal force (a force control feature), 3) free leg tip altitude smooth contact approach (to reach the ground with zero relative velocity), 4) contact point horizontal force, and 5) static stability (moving COM to a horizontal position near the rear leg tip, which is 20% of total legs' tip horizontal distance from the rare tip, as fast as possible.). Free leg pair tips' ground reaching trajectory is considered as two of our goals so as to reduce the contact velocity and make it zero to reduce normal harmful impulse and the slipping probability on the surface. $\boldsymbol{T}_{\mathrm{d}}$ and $\boldsymbol{d}_{\mathrm{d}}$ are transformation matrix for goal functions in terms of generalized coordinates, and vector of other terms in this functions' derivative respectively.

$$\begin{bmatrix} \widehat{\boldsymbol{M}}^{+}_{[8\times8]} & \boldsymbol{T}^{(\mathrm{T})}_{\mathrm{cp}[8\times2]} & \boldsymbol{0}_{[1\times5]} \\ & & -\boldsymbol{I}_{[5\times5]} \\ & & \boldsymbol{0}_{[2\times5]} \\ \boldsymbol{T}^{(\mathrm{T})}_{\mathrm{cp}[2\times8]} & \boldsymbol{0}_{[2\times7]} & \\ \boldsymbol{T}_{\mathrm{d}[5\times15]} & & \end{bmatrix}_{[15\times15]} \cdot \begin{bmatrix} \ddot{\boldsymbol{q}}_{[8\times1]} \\ \boldsymbol{\lambda}_{\mathrm{cp}[2\times1]} \\ \boldsymbol{\tau}_{[5\times1]} \end{bmatrix}_{[15\times1]} = \begin{bmatrix} \boldsymbol{d}_{\mathrm{EOM}} \\ \boldsymbol{0} \\ \boldsymbol{d}_{\mathrm{d}} \end{bmatrix}_{[15\times1]} \quad (9)$$

$$for\ (\boldsymbol{\lambda}_{\mathrm{cp}[i]} > 0\ and\ \boldsymbol{x}_{\mathrm{p[z]}} = 0),$$

Contact Model The contact release condition is represents in Eq. (9) and after each re-contact, impact equations are evaluated as in Eq. (10) again to account for state space changes. Here double contact equations are derived while for single contact $\boldsymbol{T}_{\mathrm{cp}}^{(\mathrm{T})}$ and $\boldsymbol{E}$ should be replaced for one of the leg pair tips only, and using one of the $\boldsymbol{Fht}_{\mathrm{d}}$ and $\boldsymbol{Fht}_{\mathrm{d}}$ terms (transformation matrix for front and rare leg pair tips in terms of generalized coordinates,) would be enough.

$$\begin{bmatrix} \widehat{\boldsymbol{M}}^{+}_{[8\times8]} & \boldsymbol{0}_{[8\times2]} & \boldsymbol{T}^{(\mathrm{T})}_{\mathrm{cp}[10\times4]} \\ \boldsymbol{0}_{[2\times10]} & & \\ \boldsymbol{T}_{\mathrm{cp}[4\times10]} & & \boldsymbol{0}_{[4\times2]} \end{bmatrix}_{[14\times14]} \cdot \begin{bmatrix} \dot{\boldsymbol{q}}^{+}_{[10\times1]} \\ \boldsymbol{\rho}_{[4\times1]} \end{bmatrix}_{[14\times1]} = \begin{bmatrix} \widehat{\boldsymbol{M}}^{-}_{[8\times8]} \\ \boldsymbol{0}_{[2\times8]} \\ \boldsymbol{E}_{[4\times4]} \cdot \begin{bmatrix} \boldsymbol{Fht}_{\mathrm{d}[2\times8]} \\ \boldsymbol{Rht}_{\mathrm{d}[2\times8]} \end{bmatrix} \end{bmatrix}_{[14\times8]} \cdot \dot{\boldsymbol{q}}^{-}_{[8\times1]} \tag{10}$$

Deformable Surface Model Here the goal constraints are 1) static stability 2) contact point normal force, 3) free leg tip altitude smooth contact approach, 4) contact point horizontal force, and 5) free leg tip horizontal speed smooth approach toward zero. The contact force ($\boldsymbol{qfs}$ which is a term in $\boldsymbol{q}_{\mathrm{nc}}$) is derived based on [30] which damping coefficient ($\boldsymbol{Cpc}_{(\boldsymbol{x}_{\mathrm{p}})}$) is a smooth cubic function of leg tip penetration in surface ($\boldsymbol{x}_{\mathrm{p}}$) which reaches a maximum value of $\boldsymbol{Cvs}$ for $\boldsymbol{x}_{\mathrm{p}} \geq \boldsymbol{di}$. One should notice the time dependent parameters when differentiating contact point force functions before using it as the goal function which is a little confusing (Eq. (11)). Here $\boldsymbol{Ks}$, $\boldsymbol{q}_{\mathrm{nc}}$, $\boldsymbol{rcp}$, $\boldsymbol{yzc}$, $\boldsymbol{vcp}$ and ei are surface spring characteristic, external force vectors to system in contact points and due to in-joint springs and dampers, contact point position, first contact position in the surface, and velocity vectors, and exponent of the force deformation characteristic respectively. Goal constraints on contact force vector will force the leg tip to reach the surface if it detaches from the surface.

$$\begin{bmatrix} & & \boldsymbol{0}_{[1\text{ or }2\times5]} \\ \widehat{\boldsymbol{M}}_{[8\times8]} & \boldsymbol{0}_{[8\times8]} & -\boldsymbol{I}_{[5\times5]} \\ & & \boldsymbol{0}_{[2\text{ or }1\times5]} \\ \boldsymbol{0}_{[8\times8]} & \boldsymbol{I}_{[8\times8]} & \boldsymbol{0}_{[8\times5]} \\ & \boldsymbol{T}_{\mathrm{d}[5\times21]} & \end{bmatrix}_{[21\times21]} \cdot \begin{bmatrix} \ddot{\boldsymbol{q}}_{[8\times1]} \\ \dot{\boldsymbol{q}}_{[8\times1]} \\ \boldsymbol{\tau}_{[5\times1]} \end{bmatrix}_{[21\times1]} = \begin{bmatrix} -\boldsymbol{d}_{\mathrm{EOM}[8\times1]} + \boldsymbol{q}_{\mathrm{nc}[8\times1]} \\ \dot{\boldsymbol{q}}_{[8\times1]} \\ \boldsymbol{d}_{\mathrm{d}} \end{bmatrix}_{[21\times1]} \tag{11}$$

$$\boldsymbol{qfs} = -\boldsymbol{Ks}.\left(\boldsymbol{x}_{\mathrm{p}}\right)^{ei} - \boldsymbol{Cpc}_{(\boldsymbol{x}_{\mathrm{p}})}.\begin{bmatrix} dycp \\ dzcp \end{bmatrix} \; for\; (\boldsymbol{qfs}_{[i]} > 0\; and\; \boldsymbol{x}_{\mathrm{p[z]}} \leq 0), \boldsymbol{x}_{\mathrm{p}} = \begin{bmatrix} ycp \\ zcp \end{bmatrix} - \boldsymbol{yzc}$$

Input Signal Constraints in Inverse Dynamic The input signals are updated with a delay (h) and not instantaneously by evaluating inverse dynamic so the input signal delays are modeled. Since the inputs are of velocity type, the found accelerations ($\ddot{q}_{[i]}$) are used to find input velocities ($\dot{q}_{\mathrm{d}}$) (Eq. (12)), and If input velocities tend to exceed sensor ($u_{\mathrm{lim}[i]}$) or joint physical limits ($q_{\mathrm{lim}[i]}$) in time h, then one of the goal constraints will be neglected starting from the last one (No. 5) and the corresponding joint acceleration will be constrained to remain in a safe region.

$$\dot{q}_{\mathrm{d}[i]} = \ddot{q}_{[i]} \times h + \dot{q}_{[i]} \rightarrow if: \begin{cases} \dot{q}_{\mathrm{d}[i]} \times h + \ q_{[i]} > q_{\mathrm{lim}[i]} \rightarrow \dot{q}_{\mathrm{d}[i]} = \dfrac{q_{\mathrm{lim}[i]} - q_{[i]}}{h} \\ \dot{q}_{\mathrm{d}[i]} > u_{\mathrm{lim}[i]} \rightarrow \dot{q}_{\mathrm{d}[i]} = u_{\mathrm{lim}[i]} \end{cases} \qquad (12)$$

3.2 Double Contact Phase

Despite its name, here the model may be still in single contact, however the goal constraints will differ as the free leg pair tips in previous phase reaches the surface. They are: 1 & 2) front and rear contact point normal forces, 3 & 4) front and rear contact point horizontal forces, and 5) lowering COM smoothly to stop it at 0.05 m height, for both rigid and deformable surface models. The modeling is the same as single contact model, however if both legs contact the surface, new constraint and surface force vector on second pair should be considered. In rigid model, one DOF of the system reduces and it may cause singularities in simulation. So it is not possible to impose all five constraints due to physical or sensory limitations since one of the joints cannot be considered free. Here the rear shank joint considered constrained in this case. The input signals will try to stop the joints movements if COM velocity reaches a certain small value.

4. Simulation and Results

4.1 Pre Impact Phase

Simulation assumptions and model parameters are as in table (1). Weights for the four criteria of optimizing pre landing configuration are 500, 1000 and 500 for stability index, after impact velocity vector of contact point, and harmful in-joint impulses summation. The pre configuration is 84 degrees of waist inward bending and maintaining $\pm$3 degrees absolute inclination of leg limbs. It results in a 46.9 degrees front body inclination w.r.t. contact surface for optimum landing from a 5m free fall, and the model should rotates as it falls so as to reach this configuration. As a result the rear leg pair tips contact the ground first. However after contact velocities are equal [6.3e-1, -9.84] and not zero, since all five joints reach their limiting speed of [6.2, 6.2, 6.2, -6.2, 6.2] for [qw2, qft, qfs ,qbt, qbs]. The joint between hip and rear thigh in its hip end encounters the highest impulse of 3.53e-1 Kg.m/s and the one between front body and hip in its front body end is on the second place with 3.42e-1 Kg.m/s. Contact point impulse vector is [2.47e-2, 3.39e-1] and it can be seen that maximum normal in-joint impulse is 4.1% higher than that in contact point.

4.2 Single contact Phase

In this phase it is desired to reduce normal contact force to twice the body weight for rigid surface, and become equal the model weight for the deformable surface model. These values are tuned to reach the best faceable results. Horizontal contact force is forced to become zero. Deformable surface model parameters in Table (1) are considered similar to those in [30] and [1]. As can be seen in Fig. (2 & 3), contacting foot bounces due to severe impact and front leg tip touches the ground while the other leg tip is on the fly. For the rigid and deformable surface model this phase lasts 1.2162e-01 sec and 1.2803e-01 respectively. It is showed that landing on soft surface

results in less impact impulse. Fig (2 & 3) show contact points bounced rapidly in both models, joints moved similarly and models settled on its back foot, except for rare leg tip contact and front shank angles, and landing on deformable surface caused more rare foot bending. Input signals and generated torques for model on deformable surface show more fluctuation, since the surface vibration affect the system, while the rigid surface model generates smoother input signals. Both model joints relatively followed the input signals and no major saturation or physical limitations were encountered.

In the pictures blue dotted lines are for deformable and red solid lines are for rigid surface model, and [ucpf, ucpr, ufs, uft, uw, ubt, ubs], [qcpf, qcpr, qfs, qft, qw, qbt, qbs], [Tqfs, Tqft, Tqw, Tqbt, Tqbs], [Inqfs, Inqft, Inqw, Inqbt, Inqbs], [fht, rht], [ufht, urht] and lambda Are rotational velocity (u…), relative angle (q…), input torque (T…), input signal (In…) for front leg tip, back leg tip, front shank, front thigh, waist, back thigh, and back shank, and leg tip velocity and position vectors (…ht & u…ht), and contact force vector respectively.

4.3 Double contact Phase

Here the desired forces on contact foots are 0.2 and 0.8 of body weight on front and rear leg respectively. The model generates inputs and once the COM velocity absolute value reaches 0.05 to 0.1 m/s, the stopping signal zeroes all joint velocities. The model is reported as settled once its COM absolute velocity and acceleration reaches values lower than 0.05 m/s and 0.1 m/s^2 respectively. Results are shown in Fig. (4 & 5) for simulation results and Fig. (6) for the COM velocity and accelerations trend through models' settlement. Settling duration is 0.8 for rigid surface model and 1.05 s for deformable surface model is. Fluctuations in input and torque signals of the model on deformable surface is rapid while they are smoother for the model on rigid surface. Both models tend to lean forward and the rare leg tip angles are decreased since the model front body is heavier and the least body weight should be placed on the front legs. The model on rigid surface rejected the linear momentum by bending front elbow while the other one used waist bending as the main tool for momentum rejection. As the rear leg runs into severe impulse in the first contact, both models' rare legs bounce more than the front legs before complete settlement and front leg acted as the supporting leg. Flexibility of the surface caused bouncing of front leg tip while rigidity makes rear leg bounce more. Despite the more fluctuating nature of landing on a deformable surface which will cause more control and actuation effort, the landing normal forces in this case are considerably small and not more than 1.01 of the body weight while for the rigid surface model they reach two times the body weight for supporting leg and 10 times of it for the rear bouncing leg. It is showed that energy rejection through rapid contacts occurring on a rigid surface dominates the viscos damping effect of the deformable surface model with less impacts. However the COM velocity and acceleration trend for the model on deformable surface decays smoothly while rapid changes in these graphs (Fig. (6)) for the rigid surface model can be seen. It shows that a simple mistake in steering of the landing process on a rigid surface has considerable consequences while landing maneuver on a deformable surface would be less sensitive.

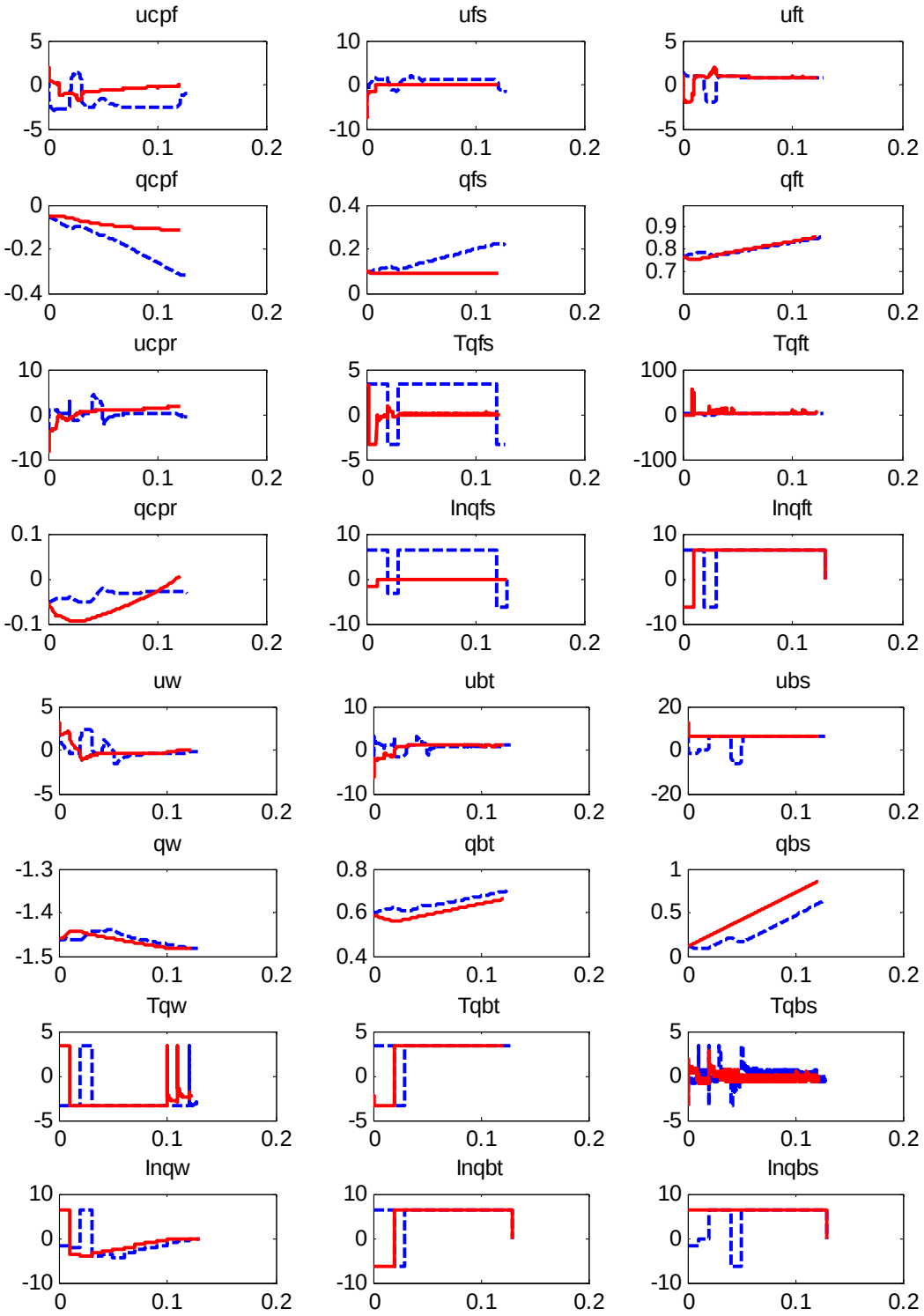

Fig. 2 Simulation results for single contact phase: blue dotted and red continues lines are for modeling on deformable and rigid surface respectively.

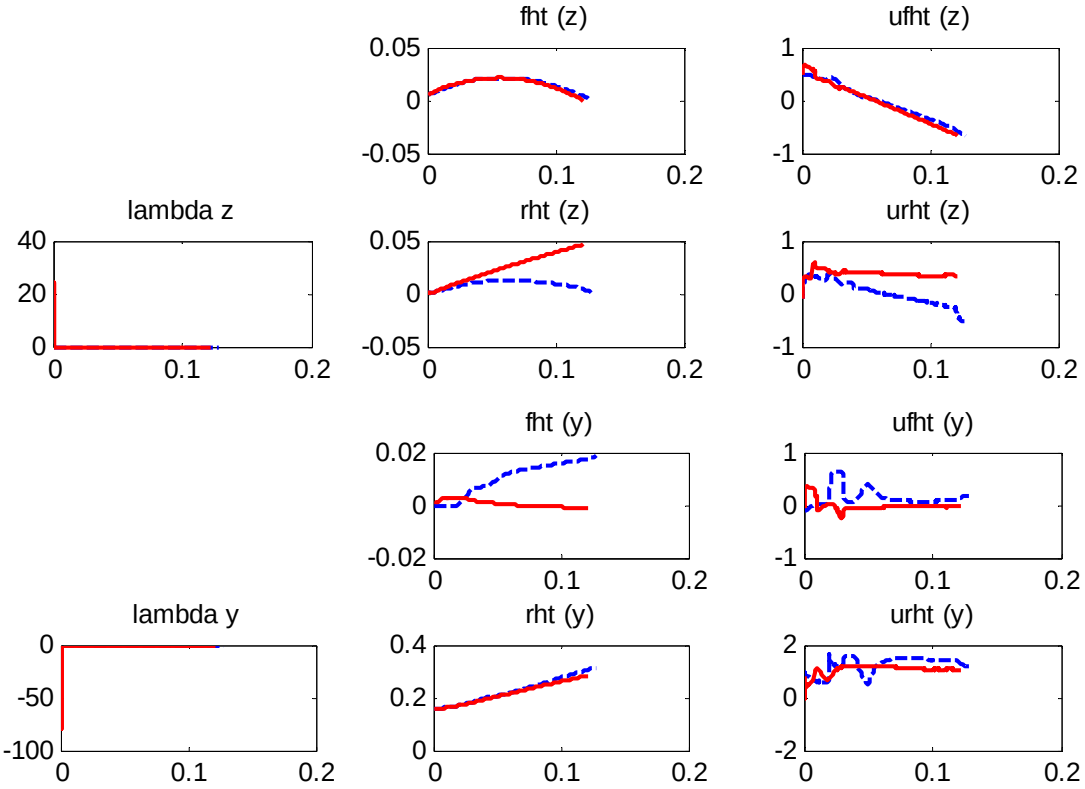

Fig. 3 Simulation results for landing single contact phase: blue dotted and red continues lines are for modeling on the deformable and rigid surface model respectively.

5. CONCLUSIONS

In this research a thorough investigation is performed on modeling, path planning and force control planning of a cat landing maneuver on two different rigid and deformable surfaces, based on a distributed 7 link 2D cat robot model. A new method for modeling called semi-flat systems in combination with mathematical approaches to deal with real word application constraints is presented. The performance of the proposed force control and path planning is showed through numerical simulations. After suggesting an optimal pre landing configuration, it is showed that different surface models change the way a set of common goals can be achieved by a single mechanism. While landing on a deformable surface produces lower instantaneous contact forces and smoother overall settlement, it needs more control effort and generates more fluctuating input signals which lead to a longer settlement time. This research suggests a combination of TMT modeling method, semi-flat dynamics for trajectory and force control planning, and intelligent switching strategy for heavily constrained systems modeling and inverse dynamic calculations as a basis of investigating complicated maneuvers such as those can in nature.

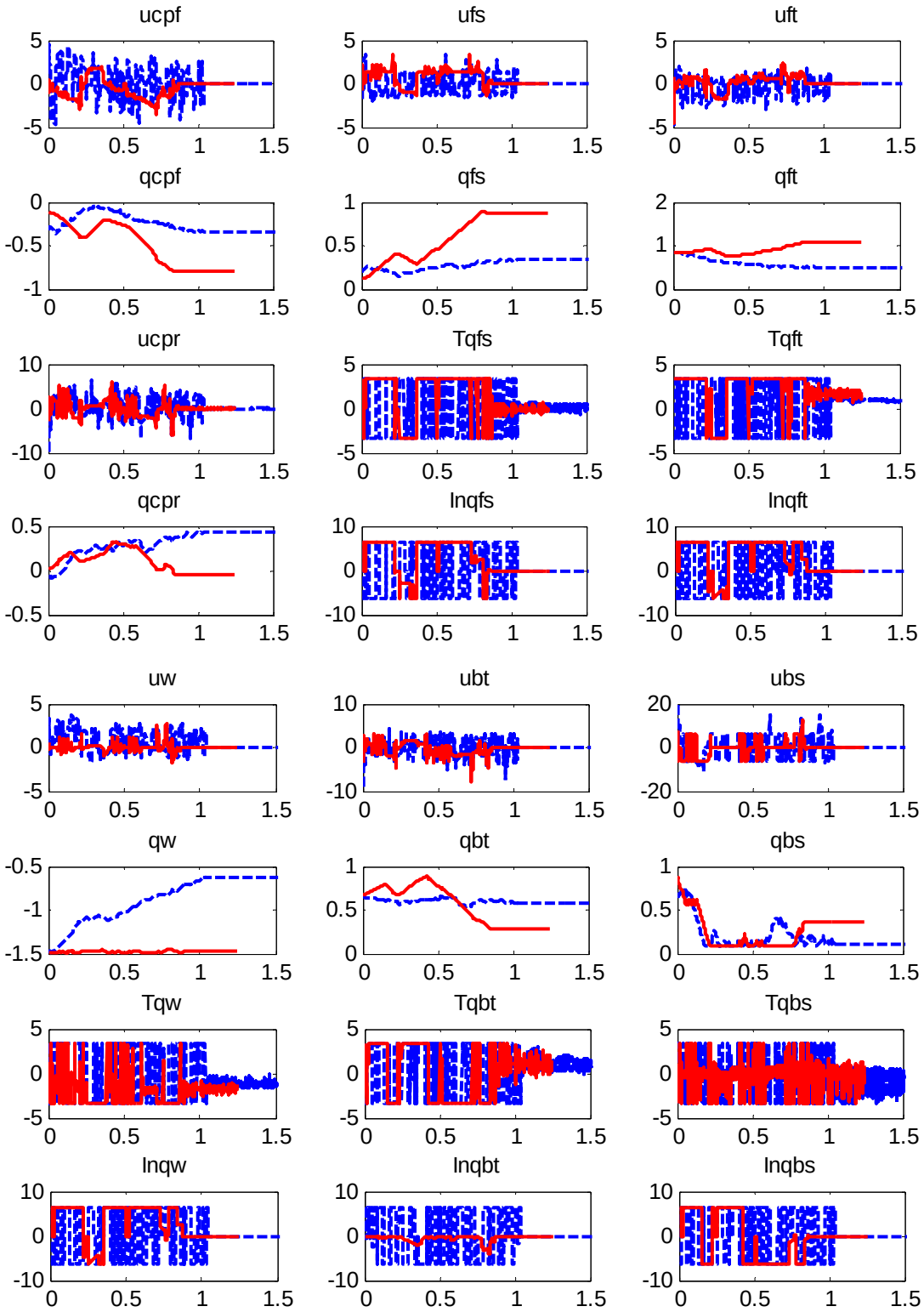

Fig. 4 Simulation results for landing double contact phase: blue dotted and red continues lines are for modeling on the deformable and rigid surface model respectively.

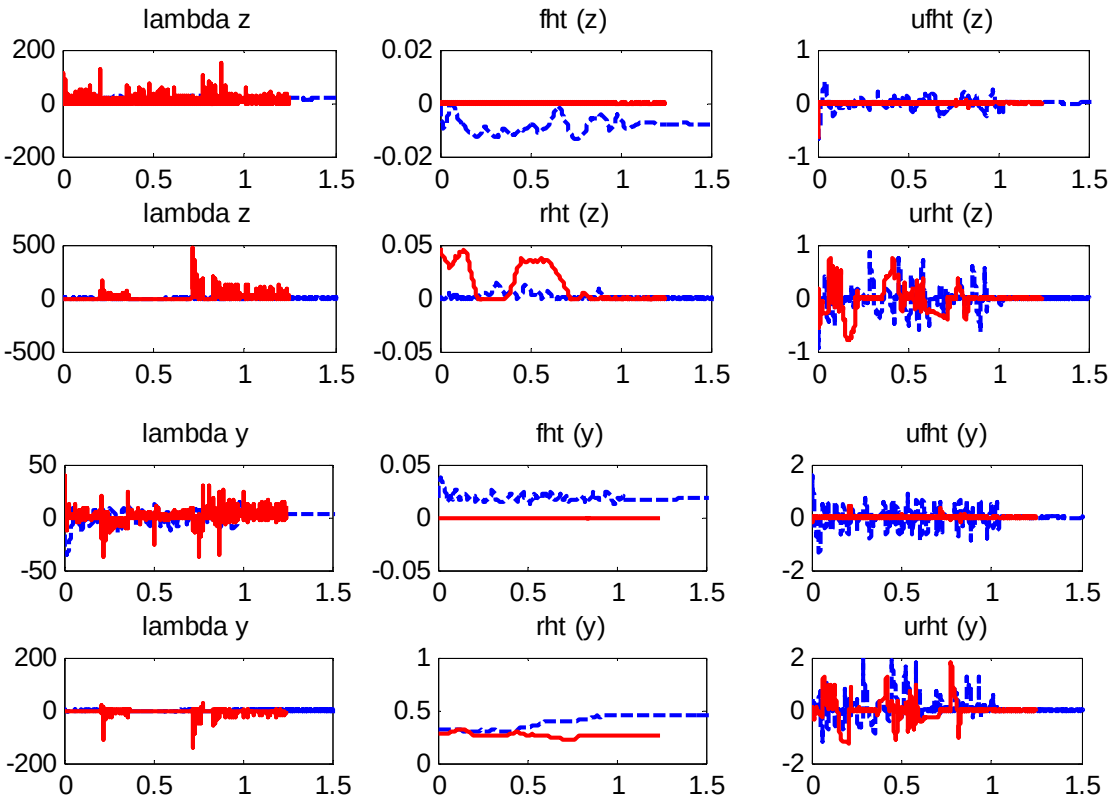

Fig. 5 Simulation results for landing single contact phase: blue dotted and red continues lines are for modeling on the deformable and rigid surface model respectively.

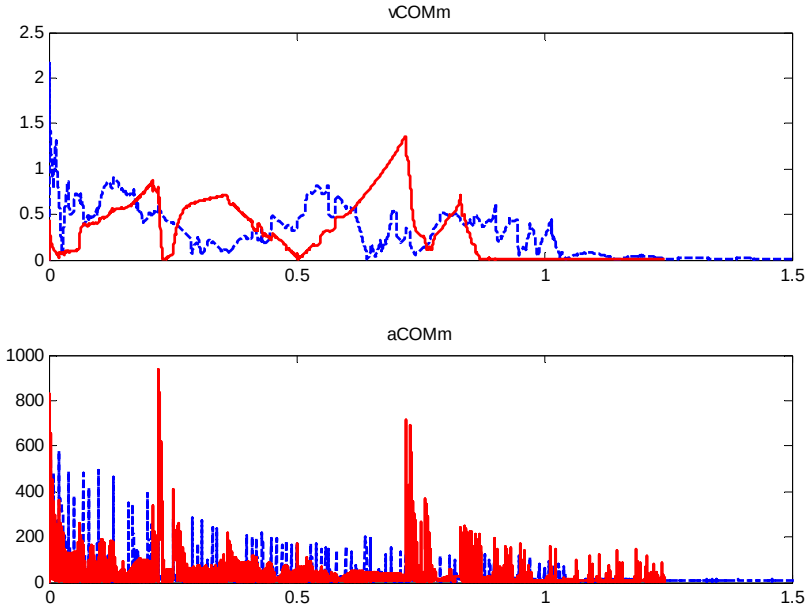

Fig. 6 Simulation results for landing double contact phase: blue dotted and red continues lines are results for modeling on the deformable and rigid surface model respectively.

Table 1. Model parameters and simulation assumptions in SI units

Sym.	Info.	Val.	Sym.	Info.	Val.	Sym.	Info.	Val.
Model Par.s						**Simulation Par.s**		
lct	Refer to Fig.1.	1.06e-1	Ich_x	Chest Inertia	8.4e-3	---	Joint Spring Coeff.	1.2
lcw		1.2e-2	Ich_y		3.2e-3	---	Joint Viscos Damping Coeff.	1.2
lhi		1.34e-1	Ich_z		7.5e-3	---	Joint Columb Damping Coeff.	0
lccy		3.4e-2	Ita_x	Tail Inertia	1.6e-4	$\boldsymbol{E}$	Coeff. of Restitution	0.05
lccz		1.37e-1	Ita_y		1.6e-4	*Ks*	Surface Spring Coeff.	2e3
lchiy		6.5e-2	Ita_z		7e-7	*Cvs*	Surface Visc. Damp. Coeff.	20
lchiz		4e-2	Iwa_x	Waist Inertia	2e-5	*ei*	Force Def. Exponent	1
mc	Chest mass	1.68	Iwa_y		1e-5	*di*	Penetration Lim. For *Cvs*	1e-2
mhi	Hip mass	6.32e-1	Iwa_z		1.4e-5	$\boldsymbol{u}_{\lim}$	Motor Speed Sensor Sat. Lim.	$\pm$6.2
mt	Tail mass	2.6e-2	$Ihip_x$	Hip Inertia	1.2e-3	$T_{\lim}$	Motor Torque lim.	1.67
mw	Waist mass	5.7e-2	$Ihip_y$		1.2e-3	*Sslim*	Torque Control Switching Lim.	0.05
			$Ihip_z$		2.5e-3	*h*	Control signal Delay	1e-2

REFERENCES

[1] Y. Sato, E. Ohashi, K. Ohnishi, in: Industrial Electronics Society, 2005. IECON 2005. 31st Annual Conference of IEEE, 2005, pp. 1821-1827.
[2] M.R. Zomlefer, R. Ho, W.S. Levine, F.E.Z. III, in, IEEE
1976, pp. 6.
[3] J.L.S.a.R.F.Z. P. A. REBACK, in, Department of Kinesiology, University of California Los Angeles, CA, 2003.
[4] T. Pfau, A. Garland de Rivaz, S. Brighton, R. Weller, Vet J, (2010).
[5] P. Przemysfaw, Sport Biomechanics, 22.
[6] A. Seyfarth, A. Friedrichs, V. Wank, R. Blickhan, Journal of Biomechanics 32 (1999) 1259-1267.
[7] C.-Y. Tse, H. Nayeb-Hashemi, A. Vaziri, P.K. Canavan, IEEE, (2011) 2.
[8] M.T. Pain, J.H. Challis, Journal of Biomechanics, 39 (2006) 119-124.
[9] W.L. Wooten, J.K. Hodgins, in: IEEE lntemational Conference on Robotics 8 Automation, IEEE, San Francisco, 2000, pp. 656-662.
[10] B.R. So, B.-J. Yi, S.-R. Oh, Y.s. Kim, in: International Conference on Intelligent Robots and systems, IEEElRSJ, Sendal, Japan, 2004, pp. 7.
[11] J.-X. Xu, Y. Sun, C.K. Pang, in: 8th IEEE International Conference on Control and Automation, Xiamen, Chinax, 2010, pp. 6.
[12] M.T.G. Pain, C. Mills, M.R. Yeadon, Journal of Biomechanics, 40 (2007) S200.
[13] M.R. Torry, C. Myers, W.W. Pennington, K.B. Shelburne, J.P. Krong, J.E. Giphart, J.R. Steadman, S.L. Woo, Knee Surg Sports Traumatol Arthrosc, 19 (2011) 653-662.
[14] M.R. Yeadon, M.A. King, S.E. Forrester, G.E. Caldwell, M.T. Pain, Journal of Biomechanics, 43 (2010) 364-369.
[15] J. McNittgray, Journal of Biomechanics, 26 (1993) 1037-1046.

[16] A. Sheets, M. Hubbard, Sports Engineering, 10 (2007) 209-220.
[17] J. Whitting, J. Steele, M. Jaffrey, B. Munro, Journal of Biomechanics, 40 (2007) S240-S240.
[18] A.E. Finch, J. Santiago, IEEE, (1996) 491-493.
[19] E. Kuo, C. Chen, T. Chen, Journal of Biomechanics, 39 (2006) 60.
[20] A. Kulasa, P. Zalewskib, T. Hortobagyib, P. DeVitab, Journal of Biomechanics, 41 (2008) 180-185.
[21] S.N. Kajita, T. ; Kaneko, K. ; Hirukawa, H., Robotics & Automation Magazine, IEEE, 14 (2007) 63-72.
[22] AshleyM.Korzun, GregoryF.Dubos, CurtisK.Iwata, BenjaminA.Stahl, J. J.Quicksall, Acta Astronautica, 66 (2010) 1146-1159.
[23] R. Niiyama, A. Nagakubo, Y. Kuniyoshi, in: International Conference on Robotics and Automation, IEEE, Roma, Italy, 2007, pp. 2546-2551.
[24] W.C.E. Wong, D.E. Orin, IEEE, (1993) 346-351.
[25] M. Yamakita, M. Kishikawa, T. Sadahiro, in: Conference on Intelligent Robots and Systems, IEEURSJ, Las Vegas. Nevada, 2003, pp. 1146-1141.
[26] Y.-D. Kim, B.-J. Lee, J.-K. Yoo, J.-H. Kim, J.-H. Ryu, in: the 2006 IEEE International Conference on Robotics and Automation, IEEE, Orlando, Florida, 2006, pp. 6.
[27] J. Ruiz-del-Solar, R. Palma-Amestoy, R. Marchant, I. Parra-Tsunekawa, P. Zegers, Robotics and Autonomous Systems, 57 (2009) 796-807.
[28] R.P. A. Chatterjee, C. K. Reddy, A. Ruina, The International Journal of Robotics Research, 21 (2002) 621-634.
[29] M. Posa, R. Tedrake, in, Massachusetts Institute of Technology, Massachusetts, 2011, pp. 15.
[30] ADAMS/Solver: C++ Functions, in: ADAMS View Help, ADAMS Software, 2012, pp. 84-87.
[31] B.-J.Y. S. H. Lee, S. H. Kim, and Y. K. Kwak., in: International Conference on Intelligent Robots and Systems, 2000, pp. 1955-1962.
[32] K. Gruber, Ruder, Denoth, J., Schneider, K.,, Journal of Biomechanics, 31 (1998) 439-444.
[33] A. Meghdar, S.M.H. Sadati, in: ASME 2013 International Design Engineering Technical Conferences & Computers and Information in Engineering Conference (IDETC/CIE 2013), Portland, Oregon, USA, 2013, pp. 1-10.
[34] T.C. John and Sandy Edminster, and Mary Smith, Sue Hall, King County, Roy J. Hostetler, DVM,, Cat Anatomy and Physiology, in: D. Michael A. Foss, Skamania County; Nancy Stewart, King County; Jean Swift, Skagit County. (Ed.), 2008.
[35] S. Kim, in, Biomimetics Robotics Lab - Massachusetts Institute of Technology, Massachusetts, 2012.
[36] S.M.H. Sadati, M. Naraghi, A.R. Ohadi, Tarbiat Modares Journal of Mechanical Engineering, 12 (2012) 52-68.
[37] W. M., v.d.L. R.Q., in, Delft, Berlin Heidelberg, 2007, pp. 15-19.
[38] M. Leonard, (1995).
[39] F. Bullo, A.D. Lewis, Geometric Control of Mechanical Systems: Modeling, Analysis, and Design for Simple Mechanical Control Systems, Springer, 2000.
[40] K. Sato, T. Iwai, Systems & Control Letters, 61 (2012) 334-342.

[41] A. Mensink, in, EEMCS / Electrical Engineering, Control Engineering, University of Twente, Twente, 2008, pp. 38.